Brown University
Division of Engineering
Providence, R.I. 02912

THREE-DIMENSIONAL TRANSIENT ANALYSIS OF A DYNAMICALLY LOADED THREE-POINT-BEND DUCTILE FRACTURE SPECIMEN

by

T. Nakamura, C. F. Shih and L. B. Freund

Division of Engineering, Brown University
Providence, RI 02912, U.S.A.

Office of Naval Research
ONR0365/3
September 1986

THREE-DIMENSIONAL TRANSIENT ANALYSIS OF A DYNAMICALLY LOADED THREE-POINT-BEND DUCTILE FRACTURE SPECIMEN

T. Nakamura*, C. F. Shih and L. B. Freund

Division of Engineering
Brown University
Providence, RI 02912 USA

ABSTRACT

A transient three-dimensional full-field analysis of a three-point-bend fracture specimen dynamically loaded into the fully yielded plastic state has been carried out. The specimen is rapidly loaded by means of a concentrated transverse force applied at mid-span on the uncracked surface of the specimen. It is assumed that the material is ductile and fracture initiation occurs after substantial plastic deformation has developed in the uncracked ligament. Furthermore it is supposed that the crack tip conditions are such that the J-integral may be adopted as a characterizing parameter. We derive an expression for the local energy flux appropriate to a three-dimensional crack front. Based on this fundamental crack tip flux integral, a domain integral representation for J which is naturally suited for the finite element method is obtained. Using the domain integral, accurate pointwise/local values of J along a three-dimensional crack front can be extracted from numerically determined field quantities. The effect of transient loading, geometry and plastic deformation on the variation of J along the crack front is examined. A purpose of the present study is to determine conditions under which the value of J at initiation may be inferred from quantities that are directly measurable in a dynamic fracture experiment. In an earlier paper a transition time was introduced to provide a practical bound on the time range over which conditions of J-dominance prevailed and the deep-crack formula was applicable under transient loadings. The transition time concept is further examined in this paper. With the full-field solutions in hand, we comment on the suitability of proposed surface locations for measurements of moment and rotation, the input measurements for application of the deep-crack formula for J. Implications for fracture testing of tough materials at relatively high loading rates are discussed.

---

*currently at Department of Mechanical Engineering, M.I.T., Cambridge, MA 02139

1. INTRODUCTION

Several experimental procedures have been recently proposed for the measurement of dynamic fracture toughness. In an earlier study [1], we carried out an analysis of a three-point-bend fracture specimen under dynamic loading, modeling a specimen that Joyce and Hackett have used to determine the fracture toughness of ductile structural steel [2]. In [1], a full-field plane strain finite element analysis is described. The crack tip values of J were computed by means of a domain integral expression and the results were compared with the estimate of J determined from the deep-crack formula proposed by Rice, Paris, Merkle [3] (with parameters appropriately replaced for the dynamic analysis). Furthermore, a notion of transition time was introduced to provide a practical bound on the time range over which conditions of J-dominance prevailed near the crack front and the deep-crack formula was applicable under transient loadings.

In order to completely understand the response of a fracture test specimen, a three-dimensional analysis is required. This is especially important if there is substantial plastic flow in the ligament of the specimen. Several analytical investigations based on three-dimensional models have been carried out for the case of quasi-static loading [4-6]. In these studies, the J-integral [7] is viewed as a paramenter characterizing the crack tip field and the determination of J as a function of position along crack front was a principal objective. The studies revealed that the variation of J along crack front is strongly dependent on the amount of plastic deformation in the uncracked ligament of the specimen.

A full-field three-dimensional finite element analysis of a dynamically loaded three-point-bend fracture specimen is presented in this paper. First a general expression for the crack tip J-integral based on the fundamental energy flux integral is given for a three-dimensional crack front in a deformable body subject to transient loadings. Then, a domain integral form of J is derived from the crack tip integral, and an expression is given for pointwise value of J along a crack front. Using the domain integral representation, accurate J values can be extracted from finite element solutions. The domain integral formulation corresponds to the method of virtual crack extension [8-11] and is particularly suited for evaluation of J in three-dimensional crack problems. For the numerical simulation, a model of the three-point-bend fracture specimen is constructed with three-dimensional finite elements. The transient finite element analysis is carried out for the time interval of interest using an explicit time integration scheme. Pertinent quantities, including J as a function of position along the crack front, are computed and recorded during the calculations. From the results, interpretations are made on the J variation along the crack front and its dependence on loading rate and elapsed time. Strong variation of field variables in the through-the-thickness direction is observed and these three-dimensional effects are assessed.

In view of the experimental procedure, the accuracy of J estimated from the deep-crack formula is evaluated by comparing estimated values with precise values extracted from the full-field solution using the domain integral expression. In addition, we will comment on the suitability of proposed surface locations for measurements of moment and rotation, these being the input measurements for appplication of the deep-crack J formula. The deep-crack expression is essentially a two-dimensional formula and we will discuss its applicability in the three-dimensional fracture problems under both quasi-static and dynamic loading conditions. The present three-dimensional analysis clarifies these and other geometrical effects associated with a standard three-point-bend fracture specimen.

2. DYNAMIC J-INTEGRAL

2.1 Energy integral for three-dimensional crack front

In the analysis of dynamic crack growth in an elastic solid under two-dimensional conditions, the dynamic energy release rate J is defined as the energy released from the body per unit crack advance. More precisely, it is the limiting value of the energy flux across a path Γ which surrounds the crack tip, divided by the instantaneous crack tip speed, as the path is shrunk onto the crack tip. A mathematical expression for the energy release rate in terms of the crack tip fields for two-dimensional problems with crack extending in the x_1-direction [12] is

$$J = \lim_{\Gamma \to 0} \int_\Gamma \left[(U+T)n_1 - \sigma_{ij} n_j \frac{\partial u_i}{\partial x_1} \right] d\Gamma \tag{2.1}$$

Here σ_{ij} and u_i are the cartesian components of stress and displacement, and n_i are the components of a unit vector normal to Γ and pointing away from the crack tip. The quantities U and T are the stress work and the kinetic energy densities, respectively, and are defined as

$$U = \int_{-\infty}^{t} \sigma_{ij} \frac{\partial^2 u_i}{\partial t' \partial x_j} \, dt' \qquad\qquad T = \frac{1}{2} \rho \frac{\partial u_i}{\partial t} \frac{\partial u_i}{\partial t} \tag{2.2}$$

To extend this idea to three-dimensional fields, suppose that the crack edge is defined in rectangular coordinates by $\xi_i(s,t)$ at any time t, where s is the arclength along the crack edge measured from some arbitrary point. The speed of the crack edge at any s is $v(s) = \sqrt{\dot{\xi}_i \dot{\xi}_i}$ and the direction of crack advance is locally $\nu_i = \dot{\xi}_i / v$ (see Fig. 1a).

Consider a tubular surface $\mathcal{S}_t$ enclosing the crack edge and moving with it. The tubular surface is formed as follows. In any plane locally perpendicular to the crack edge, specify a small crack tip contour Γ that begins on one face of the crack, encircles the crack edge, and ends on the opposite crack face. The tubular surface is completely specified by the condition that its intersection with every plane locally perpendicular to the crack edge is the same curve Γ at any time t (see Fig. 1c).

For a crack advancing under three-dimensional conditions, at any instant of time the energy flux through the tubular surface $\mathcal{S}_t$ is

$$F(\mathcal{S}_t) = \int_{\mathcal{S}_t} \left[(U+T)\dot{\xi}_i n_i + \sigma_{ij} n_j \dot{u}_i \right] d\mathcal{S}_t \tag{2.3}$$

where n_i are the components of the unit normal vector to $\mathcal{S}_t$ directed away from the crack edge and other quantities are as defined above. At any point on $\mathcal{S}_t$, the particle velocity $\dot{u}_i$ may be separated into two contributions, one arising from the fact that u_i is changing at the fixed point on $\mathcal{S}_t$ and a

convected contribution arising from the fact that this point is moving through material where u_i has a spatial gradient. Thus,

$$\dot{u}_i = \left.\frac{\partial u_i}{\partial t}\right|_{\mathcal{S}_t} - \frac{\partial u_i}{\partial x_j}\dot{\xi}_j \tag{2.4}$$

Therefore, if $s_a \leq s \leq s_b$ is the range of arclength along the crack edge, then

$$F(\mathcal{S}_t) = \int_{s_a}^{s_b} v(s) \int_\Gamma \left[(U+T)\nu_k n_k - \sigma_{ij} n_j \frac{\partial u_i}{\partial x_k}\nu_k\right] d\Gamma\, ds \tag{2.5}$$

where $d\Gamma$ is that part of the tube between s and $s+ds$. The asymptotic relation, $\dot{u}_i \sim -(\partial u_i/\partial x_j)\dot{\xi}_j$ as $r \to 0^+$, has been invoked in (2.5) [12]. The quantity $v(s)$ is the local crack advance per unit time, so that the integral multiplying it is the energy flow per unit crack advance through $d\Gamma$. The local energy release rate is

$$J(s) = \nu_k \lim_{\Gamma\to 0} \int_\Gamma \left[(U+T)n_k - \sigma_{ij} n_j \frac{\partial u_i}{\partial x_k}\right] d\Gamma \tag{2.6}$$

The direction of crack advance ν_k depends only on s and is taken out of the integration. Under quasi-static conditions and where U is taken to be the strain energy function, the integral to the right of ν_k is the so-called J_k conservation integral [13,14]. A unified treatment of crack tip integrals and conservation/dissipation integrals as direct consequences of appropriate balance laws can be found in [15].

Suppose that over an arbitrarily small increment of time, the crack front at s advances by $\lambda(s)$ in the normal direction (in the plane of the crack) within the segment $s_a \leq s \leq s_b$. With respect to the reference coordinate system, the crack growth increment is $\lambda(s)\nu_k(s)$ which is more conveniently denoted by $l_k(s)$ as depicted in Fig 1b. Associated with this increment of growth of crack front, the total energy released by the body is

$$\overline{J} = \int_{s_a}^{s_b} J(s)\lambda(s)\, ds = \lim_{\Gamma\to 0} \int_{\mathcal{S}_t} \left[(U+T)n_k - \sigma_{ij} n_j \frac{\partial u_i}{\partial x_k}\right] l_k\, dS \tag{2.7}$$

where $dS = d\Gamma ds$. The energy released through different segments of the crack front is obtained from (2.7) by appropriate choice of s_a and s_b.

For quasi-static monotonic loading conditions and proportional stress history at each material point, the integral (2.1) is path independent for a nonlinear elastic or elastic-plastic material, and the value of J does not depend on the limiting process of shrinking the contour Γ onto the crack tip. In this case, the integral is precisely Rice's J-integral [7] and its value is the amplitude of near crack tip field. Under dynamic loading conditions, inertial effects preclude the definition of an equivalent path independent integral and the value of the near tip field intensity must be expressed

in terms of the crack tip limit in (2.1), although the shape of the contour as shrunk onto the crack tip is arbitrary. For a 3-D crack front, the local/pointwise value of J is only defined in terms of the limit in (2.6).

2.2 Domain integral representation for J

It is apparent that from a discrete computational point of view, the expression (2.6) is not suitable for evaluating values of $J(s)$ nor is (2.7) useful for evaluating values of $\overline{J}$. As in the two-dimensional case, accurate evaluations of field near the crack front is difficult and alternate forms for $\overline{J}$ that are better suited for numerical calculations are discussed here. The finite domain form for $\overline{J}$ follows directly from the fundamental crack tip energy integral (2.7) by the application of the divergence theorem over part of the cracked solid. The present derivation follows the formulation in [6,11] where it is presented in greater detail.

Let $\mathcal{S}_o$ be an arbitrary outer surface (including the end-caps) which surrounds the inner tubular surface $\mathcal{S}_t$ as depicted in Fig. 1c. The connecting upper and lower crack faces are $\mathcal{S}_+$ and $\mathcal{S}_-$. Thus $\mathcal{S}$ ($\mathcal{S} = \mathcal{S}_o + \mathcal{S}_t + \mathcal{S}_+ + \mathcal{S}_-$) is a closed surface. To write (2.7) as an integral over a closed and an integral over physical boundaries (i.e. $\mathcal{S}_+ + \mathcal{S}_-$) we introduce a weighting function q_k. The vector q_k is a smooth function of x_1, x_2 and x_3 subject to these restrictions. It is equal to $l_k(s)$ on $\mathcal{S}_t$, vanishes on $\mathcal{S}_o$ and varies in an appropriate manner (to be specified) along the crack faces. With q_k so defined, the integral in (2.7) can be written as an integral over the closed surface $\mathcal{S}$ and an integral over the physical boundaries $\mathcal{S}_+ + \mathcal{S}_-$,

$$\begin{aligned}\overline{J} = \lim_{\Gamma\to 0}\int_{\mathcal{S}}\left[\sigma_{ij}\frac{\partial u_i}{\partial x_k} - (U+T)\delta_{jk}\right]m_j q_k\, d\mathcal{S} \\ - \lim_{\Gamma\to 0}\int_{\mathcal{S}_+ + \mathcal{S}_-}\left[\sigma_{ij}\frac{\partial u_i}{\partial x_k} - (U+T)\delta_{jk}\right]m_j q_k\, d\mathcal{S}\end{aligned} \tag{2.8}$$

Here m_j is the unit normal on $\mathcal{S}$ that points away from the enclosed volume. On the surface $\mathcal{S}_t$, m_j is the negative of n_j which has been defined earlier. On each of the crack faces, q_k is prescribed to be orthogonal to m_k (i.e. $q_k m_k = 0$ on $\mathcal{S}_+$ and $\mathcal{S}_-$). In addition if crack faces are traction free, the integral over $\mathcal{S}_+ + \mathcal{S}_-$ in (2.8) vanishes identically.

We apply the divergence theorem to the closed integral in (2.8) and invoke the balance of linear

momentum to get the following finite domain representation

$$\overline{J} = \int_V \left[\sigma_{ij} \frac{\partial u_i}{\partial x_k} \frac{\partial q_k}{\partial x_j} - (U+T) \frac{\partial q_k}{\partial x_k} + \rho \left(\frac{\partial^2 u_i}{\partial t^2} \frac{\partial u_i}{\partial x_k} - \frac{\partial u_i}{\partial t} \frac{\partial^2 u_i}{\partial x_k \partial t} \right) q_k \right. \\ \left. + \left(\sigma_{ij} \frac{\partial^2 u_i}{\partial x_j \partial x_k} - \frac{\partial U}{\partial x_k} \right) q_k \right] dV \tag{2.9}$$

In the above equation, crack faces are assumed to be traction free. If crack face traction cannot be neglected, the second integral in (2.8) must be appended to the integral in (2.9). The inclusion of traction on crack faces and body force like terms are discussed in greater detail in [6]. In (2.9), the domain V has been taken to be the *total* volume enclosed by the arbitrary outer surface $\mathcal{S}_o$, including the crack tip region. Any difference between the integration over the volume V and the volume enclosed within $\mathcal{S}$ vanishes as $\mathcal{S}_t$ is shrunk onto the crack front. It may be noted that the last two terms in (2.9) cancel identically in the case of an elastic solid.

We emphasize that any smooth (C^o) function which is appropriately defined within the enclosed volume (i.e. the function assume the precribed values on surfaces $\mathcal{S}_t$, $\mathcal{S}_o$ and crack faces $\mathcal{S}_+$, $\mathcal{S}_-$) could serve as the weighting function q_k. The vector function $q_k(x_1, x_2, x_3)$ may be interpreted as the virtual translation of material point (x_1, x_2, x_3) in V due to virtual extension of the crack front by $l_k(s)$ [6,8-11]. Since $\mathcal{S}_o$ is an arbitrary outer surface, the value of $\overline{J}$ does not depend on the size or shape of the arbitrary volume V enclosed by $\mathcal{S}_o$. This property of the domain representation provides a useful check on the consistency and quality of the numerical solution.

An approximation of the value of $J(s)$ is obtained by assuming that it is constant in an interval $s_a < s < s_b$. The crack front is then perturbed in this interval, say an amount $\lambda(s)$ in the plane of the crack, where $\lambda(s) = 0$ outside of the interval. This perturbation of the crack front results in a total energy release rate $\overline{J}$ according to (2.9). Then $J(s)$ is given by

$$J(s) = \overline{J} \Big/ \int_{s_b}^{s_a} \lambda(s)\, ds \tag{2.10}$$

A more precise scheme for calculating $J(s)$ which is also consistent with the finite element formulation is discussed in Section 4.2.

2.3 Specialization to a stationary crack front

For the case of stationary crack tip in a dynamically loaded body, the kinetic energy is bounded at the crack tip and consequently it makes no contribution to (2.1). The energy release rate for

this case is

$$J = \lim_{\Gamma \to 0} \int_{\Gamma} \left(U n_1 - \sigma_{ij} n_j \frac{\partial u_i}{\partial x_1} \right) d\Gamma \tag{2.11}$$

Similarly the expression for the local energy release rate at the point s on the three-dimensional crack is

$$J(s) = \lim_{\Gamma \to 0} \int_{\Gamma(s)} \left(U n_k - \sigma_{ij} n_j \frac{\partial u_i}{\partial x_k} \right) \nu_k \, d\Gamma \tag{2.12}$$

The specialization of (2.9) to a stationary crack front in a dynamically loaded body is

$$\overline{J} = \int_V \left(\sigma_{ij} \frac{\partial u_i}{\partial x_k} \frac{\partial q_k}{\partial x_j} - U \frac{\partial q_k}{\partial x_k} + \rho \frac{\partial^2 u_i}{\partial t^2} \frac{\partial u_i}{\partial x_k} q_k \right) dV \tag{2.13}$$

It may be noted that (2.13) can be derived directly from (2.12) using the procedure which led to the integral in (2.9). A method, based on the expression (2.13), for extracting accurate values of the intensity of near tip stresses and deformation from the fields determined from numerical simulation will be presented in Section 4.

To arrive at the expression (2.13), U is taken to be a potential function for stress, i.e.,

$$\sigma_{ij} = \frac{\partial U}{\partial \epsilon_{ij}} \tag{2.14}$$

Here ϵ_{ij} are the cartesian components of strain. In the case of a solid whose mechanical response is described by a stress-strain relationship of incremental type, the stress work density is dependent on strain history and (2.14) generally does not apply. However, when certain conditions are met any deviation from the equality is very small and can be neglected. The conditions require the load applied to the crack tip region to be monotonically increasing and stress histories for material particles to be nearly proportional [16].

3. J ESTIMATES FOR TRANSIENT PROBLEMS

3.1 Transition time

The dynamically loaded three-point-bend specimen has been proposed for the measurement of dynamic fracture toughness [2]. A schematic of the specimen is shown in Fig. 2a. The specimen has a through-thickness planar crack of length a (the crack front being parallel to the x_3-axis) and is supported by rollers seperated by a distance of $2L$. A dynamic load P is applied on the surface $x_1 = 0$ at the center span. In [1], we introduced a transition time t_T to provide an estimate of the time beyond application of the loading at which a J-dominated field is established in the crack tip region and a deep-crack J-formula is applicable. We assumed that an estimate of the transition time can be determined from the time history of the relative magnitudes of the total kinetic energy and the total deformation energy (or stress work) of the specimen. In particular, the transition time is defined as the time beyond which the kinetic energy of the specimen is less than the energy of deformation.

Direct measurement of the total kinetic and deformation energies in a laboratory specimen is not possible. However, these quantities can be approximated by considering simple models consistent with actual boundary measurements. In [1] an estimate of the kinetic energy was obtained by means of a model based on elastic Bernoulli-Euler beam theory with an assumption that the kinetic energy at the early stage is dominated by elastic structural response. To approximate the deformation energy, a quasi-static elastic 2-D three-point-bend model was considered. For this model, the relationship between the total strain energy of the specimen and the displacement at the load point is known. Using these models, the ratio of kinetic energy to deformation energy at time t is given in terms of the deflection $\Delta(t)$ and the velocity $\dot{\Delta}(t)$ at the load-point; these quantities are of particular interest since they can be measured in a dynamic fracture experiment. Specifically,

$$\left(\frac{K}{W}\right)_{\text{model}} = \left(S\,\frac{H}{c_o}\,\frac{\dot{\Delta}(t)}{\Delta(t)}\right)^2 \tag{3.1}$$

Here H is the width of the specimen, c_o is the sound speed in the specimen (i.e., longitudinal bar wave speed) and the (time-independent) dimensionless shape factor S depends on the dominant mode shape and elastic compliance C_S of the specimen. For a bend specimen of thickness B and span $2L$ between supports as shown in Fig. 2a, S is given by

$$S = \left(\frac{L\,B\,E\,C_S}{H}\right)^{\frac{1}{2}} \tag{3.2}$$

where E is the Young's modulus. The values of S for a standard ASTM three-point-bend specimen

is given in [1]. In the above model analysis the effect of discrete stress waves was ignored. Obviously, the values of estimated energies are not valid until after elastic waves make several passes within the specimen. The limitation is of no consequence since such wave effects are unimportant at the transition time. The model analysis also assumed that effect of plastic deformation is not significant prior to the transition time.

For the purpose of writing an explicit expression for t_T we introduce a dimensionless displacement coefficient D defined by

$$D = \left. \frac{t\ \dot{\Delta}(t)}{\Delta(t)} \right|_{t_T} \tag{3.3}$$

For example, if the time variation of the displacement can be represented by $\Delta = \beta\ t^{\gamma}$ then $D = \gamma$. With t_T defined as the time when the ratio K/W is equal to unity, we combine (3.1) and (3.3) to get [1]

$$t_T\ =\ D\ S\ \frac{H}{c_o} \tag{3.4}$$

To evaluate the accuracy of the estimate of the transition time based on (3.1) the finite element results for the dynamically loaded bar is employed. The details of the finite element model and calculations are given in Section 5. With $\Delta(t)$ and $\dot{\Delta}(t)$ obtained from the results of the 3-D finite element calculations, and values of S, H and c_o appropriate to the specimen, we calculated the time variation of the ratio K/W according to (3.1). The ratio of the actual total kinetic and deformation energies from the finite element model (obtained by summing the respective energies over all the elements) is also calculated. Both ratios are plotted in Fig. 3. The close agreement between the curves is evidence of the accuracy of the estimate of relative energy levels based on the elementary model analysis from which (3.1) which was derived. During the early stages of the transient, the kinetic energy dominates. With progress of time deformation energy (stress work) dominates. The ratio K/W computed by (3.1) decreases to unity, at time $t_T c_1/H \simeq 28$ (or $t_T c_o/H \simeq 24$) in dimensionless units. Here c_1 is the longitudinal wave speed in an unbounded medium and H/c_1 is the time it takes the wave to travel the specimen's width. It is worth noting that the transition time determined from a 2-D analysis is $t_T c_1/H \simeq 27$ [1]. We point out that nearly identical estimates of the transition time are obtained upon replacing $\dot{\Delta}(t)/\Delta(t)$ by $\dot{\theta}_L(t)/\theta_L(t)$ in (3.1) where $\theta_L(t)$ is the specimen rotation about a hinge axis at the ligament. The precise definition of $\theta_L(t)$ is given in the next section.

In summary, we observe that the response of specimen can be conveniently characterized by a short-time response dominated by discrete waves and a long-time response dominated by deformation energy. At the transition time structual inertial effects are important. Beyond the transition time, inertial effects diminishes relative to the overall energy absorbed by the body.

3.2 The deep-crack estimation procedure

On the basis of transient 2-D finite element analyses a formula for the computation of dynamic J from measurable quantities was proposed in [1]. The formula is a modified version of a deep-crack formula for calculating the value of J under essentially equilibrium conditions [3]. Under high-rate of loading, the inertial resistance of the specimen screens the crack tip region from the applied loads. To minimize this effect, the variables in the quasi-static formula are replaced by equivalent variables which characterize the near crack region of the body. Thus the moment is taken to be the net moment M_L carried by the ligament, and the corresponding rotation is replaced by the crack mouth opening displacement divided by the distance between the crack mouth and the hinge axis on the ligament and is denoted by θ_L. With these changes, the formula

$$J_{dc}(t) = \frac{2}{bB} \int_0^{\theta_L(t)} M_L(t')\, d\theta_L(t') \tag{3.5}$$

is proposed for estimating the value of J in a dynamically loaded three-point-bend ductile fracture specimen. In the above expression, b is the ligament length and B is the specimen thickness. At the level of beam approximation, the integral of the moment and angle in (3.5) represents the work done on the ligament. We employ the subscript dc on J to distinguish estimates based on the assumption of deep-crack from precise values based on (2.13).

3.3 Inferred rotation and moment at the ligament

To calculate $J_{dc}(t)$ according to (3.5), the values of $\theta_L(t)$ and $M_L(t)$ must be known. In an experiment, the angle θ_L can be determined from the measurement of the crack mouth opening displacement δ and an estimate of the hinge axis location necessary to convert this displacement to a rotation. The opening displacement at the crack mouth is essentially constant through the thickness. Thus δ is a well-defined measurable quantity. The hinge axis is an effective line on the ligament plane (and parallel to the x_3-axis) where the axial strain (and stress) vanishes. The determination of the hinge axis from the full-field solution will be taken up in Section 4.3. Under fully yielded conditions, the hinge axis can be rather accurately estimated using the Green and Hundy plane strain slip-line solution [17] for a rigid-perfectly plastic material. The rotation about the ligament based on the latter hinge axis is denoted by θ_L^*.

The direct measurement of the net moment M_L carried by the ligament is extremely difficult, due in part to severe plastic deformation between the load-point and the crack tip. Furthermore the three-dimensional nature of the deformation fields near the crack tip and in the vicinity of the ligament preclude the use of surface measurements in these regions for the determination of the net

moment carried by the uncracked ligament. Thus it appears the instantaneous values of M_L must be inferred from measurements of the moment and the shear force at some distance away from the cracked section and from the roller support. At a location remote from the cracked section and the roller support, (e.g. the section mid-way between the crack plane and the roller support), the section should remain elastic and the fields should not vary through the thickness. Indeed results from 3-D finite element calculations which are discussed in Section 5 support the above description of the fields. Thus the bending moment M_R and the shear force S_R acting on the tranverse plane at the remote location can be accurately measured by means of strain gauges on the surface of the specimen. Denoting the value of the moment on the ligament as inferred from the measurements at the remote surface location by M_L^*, overall quasi-static equilibrium requires that

$$M_L^* = M_R + S_R L_R \tag{3.6}$$

where L_R is the distance of the remote section along the beam from the cracked section. Since the remote section being considered is about the mid-way between the cracked section and the roller support, M_R and $S_R L_R$ will be of comparable magnitude.

In a dynamic fracture experiment, the inertial response of the material between the cracked section and the remote section must be included in (3.6). Such inertial contribution has been included in the analysis in [1]. However if the time to fracture initiation is greater than the transition time, the inertial contribution is small and M_L^* as given by (3.6) is the appropriate moment for use in the computation of J_{dc}.

4. NUMERICAL PROCEDURE

The full-field 3-D numerical simulation has several objectives. It will be shown that under dynamic conditions, the local value of J at points along the crack front can be accurately calculated using the finite domain (volume) integral representation (2.13). We then examine the effect of transient loading, geometry and plastic deformation on the variation of J along the crack front. The usefulness of of the transition time concept and the accuracy of the deep-crack J formula (3.5) based on measurable load and deformation histories will be assessed. Finally the suitablity of proposed surface measurements for the determination of J will be clarified.

4.1 Finite element procedure

The duration of the event of interest relative to the time for wave passage through the structure is the important consideration in the choice of an integration scheme for a dynamic analysis. Our primary interest is the response of a cracked specimen under impact load over a time span which is large compared to the time for the wave to travel the length of the specimen. However we are also interested in the dynamic response of the specimen near the transition time when the discrete stress waves may still be important. An accurate resolution of fields at early time require that small time steps be taken. Comparisons of relative efficiency of explicit and implicit schemes have shown that three-dimensional numerical simulations of dynamic problems can be more econcomically carried out using explicit schemes [18]. Even if the higher frequencies are not of interest, the large bandwidth that arises from a 3-D model and the overhead connected with an out-of-core solver will render an implicit scheme ineffective. Guided by these considerations, we employed a lumped mass explicit integration scheme for all our calculations. The resulting discrete equations of motion are uncoupled and the nodal accelerations are obtained by trivial inversion of the diagonal mass matrix. Our numerical experimentations suggest that the 8-node hexahedron element is optimal for the intended numerical study. All numerical results reported in this paper were obtained using a modified version of the finite element program FEAP [19].

To alleviate potential numerical difficulties associated with deformation into the fully yielded plastic state, we employ the so-called B-bar method for the formation of the stiffness matrices [20,21]. In the case of the 8-node trilinear hexahedron element, the volumetric components of B are obtained by 1-point quadrature while the deviatoric components are obtained by the $2 \times 2 \times 2$ quadrature rule. The former integration results in a uniform hydrostatic pressure throughout the element. As a safequard against spurious pressure mode, the modified $\overline{\mathrm{B}}$ matrix [1] is the normalized

sum of the $\overline{\mathrm{B}}$ matrix given in [21] and the regular B matrix [22]:

$$\overline{\mathrm{B}} = \mathrm{B}^{\mathrm{dev}} + \overline{\mathrm{B}}^{\mathrm{vol}} + \epsilon\,(\mathrm{B}^{\mathrm{vol}} - \overline{\mathrm{B}}^{\mathrm{vol}}) \qquad 0 \le \epsilon \le 1 \tag{4.1}$$

The regular B matrix is recovered from (4.1) by setting $\epsilon = 1$ while the $\overline{\mathrm{B}}$ matrix in [21] is obtained for $\epsilon = 0$. In our analysis, $\epsilon = 0.05$ was used.

4.2 Discrete formulas for the evaluation of J

The discrete form of $\overline{J}$ (2.13) based on $2 \times 2 \times 2$ Gaussian quadrature appropriate to the 8-node linear hexahedron element is

$$\overline{J} = \sum_{\substack{\text{all elements} \\ \text{in V}}} \sum_{p=1}^{8} \left\{ \left[\sigma_{ij} \frac{\partial u_i}{\partial x_k} \frac{\partial q_k}{\partial x_j} - U \frac{\partial q_k}{\partial x_k} + \rho \frac{\partial^2 u_i}{\partial t^2} \frac{\partial u_i}{\partial x_k} q_k \right] \det \left[\frac{\partial x_m}{\partial \eta_m} \right] \right\}_p w_p \tag{4.2}$$

Here the field quantities including q_k and its spatial derivatives are evaluated at quadrature points ($p = 1, 2, \ldots, 8$) and weighted by w_p and the determinant of the Jacobian matrix $\det(\partial x_m / \partial \eta_m)$ [22]. The acceleration $\partial^2 u_i / \partial t^2$ at quadrature points are obtained from nodal values using the trilinear interpolation function. To maintain consistency with the isoparametric formulation, the values of q_k and $\partial q_k / \partial x_i$ at the quadrature points are evaluated from

$$q_k = \sum_{I=1}^{8} N_I Q_{kI} \qquad \frac{\partial q_k}{\partial x_i} = \sum_{I=1}^{8} \sum_{k=1}^{3} \frac{\partial N_I}{\partial \eta_m} \frac{\partial \eta_m}{\partial x_i} Q_{kI} \tag{4.3}$$

Here N_I is the trilinear shape function and Q_{kI} is the value of q_k associated with the I^{th} local node of an element. Nodal values Q_{kI} can be assigned in accordance with any smooth function as long as the appropriate values for q_k on $\mathcal{S}_t$, $\mathcal{S}_o$, $\mathcal{S}_+$ and $\mathcal{S}_-$ are obtained (see Section 2.2). Numerical experimentations have shown that the value of $\overline{J}$ is insensitive to the choice of Q_{kI}. Thus mesh design and convenience are the only considerations in selecting smooth functions for generating the values Q_{kI}. A more detail discussion of various aspects of the implementation of the domain representation of J has been given in [6,11].

The value of J at a nodal point (or the function $J(s)$ along the crack front) can be determined in the following manner. We consider the M^{th} line segment which includes the M^{th} node on the crack front. The line segment begins and ends on the nodes $M-1$ and $M+1$ at s_a^M and s_b^M respectively. Points on the segment advances by $\lambda_M(s)$ (in the normal direction in the plane of the

crack). In terms of the present variables, the energy released by the body (2.7) is written as

$$\overline{J}_M = \int_{s_a^M}^{s_b^M} J(s)\,\lambda_M(s)\,ds \tag{4.4}$$

Here $\overline{J}_M$ is the energy release computed by the domain integral expression (4.2). We assume that the local energy release rate, $J(s)$, is a continuous function of s and can be represented in the form

$$J(s) = \sum_{L=1}^{\mathrm{N_C}} N_L(s)\,J_L \tag{4.5}$$

where $\mathrm{N_C}$ is the total number of nodes on the entire crack front, $N_L(s)$ is the basis function consistent with the finite element shape function and J_L is the value of J at the L^{th} node on the crack front. Since the crack front region is modeled by 8-node trilinear elements, $N_L(s)$ is a piecewise linear function of s. Similarly the function $\lambda_M(s)$ has the form

$$\lambda_M(s) = \sum_{L=1}^{\mathrm{N_C}} N_L(s)\,\lambda_M^L \tag{4.6}$$

where λ_M^L is the crack advance at the L^{th} node on the crack front. The total number of segments advanced in this manner is equal to the total number of nodes on the crack front $\mathrm{N_C}$. By requiring λ_M^L be equal to unity for $L = M$, and λ_M^L be zero for $L \neq M$, (4.6) simplifies to

$$\lambda_M(s) = N_M(s) \tag{4.7}$$

Substituting (4.5) and (4.7) in (4.4), we have

$$\overline{J}_M = \sum_{L=1}^{\mathrm{N_C}} J_L \int_{s_a^M}^{s_b^M} N_L(s) N_M(s)\,ds \tag{4.8}$$

We repeat the above procedure for every node on the crack front to obtain a system of N_C linear equations for N_C unknown J_L's. The value of J_L is given by the solution to (4.8), i.e.,

$$J_L = \sum_{M=1}^{\mathrm{N_C}} A_{LM}^{-1}\,\overline{J}_M \qquad \text{where} \qquad A_{LM} = \int_{s_a^M}^{s_b^M} N_L(s) N_M(s)\,ds \tag{4.9}$$

Since the basis function $N_L(s)$ spans over three nodes on the crack front, A_{LM} has a bandwidth of three. With values of J_L in hand, the value of J at any point s on the crack front is obtained from (4.5).

The value of J_L can also be obtained by appealing to the approximation (2.10) for $J(s)$. With this approximation, the J at a node is uncoupled from the $J's$ at the other nodes on the crack front, i.e.,

$$J_L = \overline{J}_L \Big/ \int_{s_a^L}^{s_b^L} N_L(s)\, ds \tag{4.10}$$

If $\overline{J}_M$ varies smoothly along the crack front, J_L as computed by (4.10) differs negligibly from its more accurate value determined by (4.9). However if a particular nodal value is evaluated inaccurately (e.g. the J value at a node on a free surface), the inaccuracy can have an adverse effect on the values of J at the neighboring nodes if (4.9) is used. The inaccuracy is confined to the particular node if (4.10) is used.

The average value, pertaining to the entire crack front, is obtained by integrating $J(s)$ over the entire crack front and dividing the resulting value by the total length of crack front. This value, denoted by J_{ave}, may also be determined directly from (4.2). In this calculation, a unit virtual extension of the entire crack front (take $\lambda(s) = 1$ for all the nodes on the crack front) is imposed and the resulting value of $\overline{J}$ is divided by the crack front length to give J_{ave}. We note that the two methods of computing J_{ave} are equivalent.

4.3 Calculations of moments and rotations

The moment carried by the uncracked ligament M_L is required in the deep-crack formula (3.5) for estimating J. The moment is calculated from the forces acting on the plane of the ligament. On the symmetry plane $x_2 = 0$, the nodal forces (normal to the symmetry plane) acting on nodes which are positioned at the same x_1 coordinate are summed (each row of nodes being parallel to the x_3-axis) to give the resultant normal nodal force on that row. This is repeated for every row of nodes on the ligament plane. The location where the linearly interpolated resultant nodal force changes its sign is taken as the effective hinge axis. Suppose the effective hinge axis (a line parallel to the x_3-axis) is directed along $x_1 = h_L$. The moment carried by the ligament plane, $0 \le x_1 \le b$ and $-B/2 \le x_3 \le B/2$, is given by

$$M_L = 2 \sum_{i=1}^{N_L} {f_2}^i ({x_1}^i - h_L) \tag{4.11}$$

Here N_L is the total number of nodes on the half-ligament plane, ${f_2}^i$ is the nodal force and ${x_1}^i$ is the x_1 coordinate of the i^{th} ligament node. In writing (4.11) we have taken advantage of the symmetry condition on the plane $x_3 = 0$.

The inferred moment carried by the ligament (3.6) is determined from the stresses given by

the strip of elements near the free surface at $x_3 = B/2$ at the quarter-span. These element values should be representative of surface measurements taken in experiments. To facilitate the moment computations, the elements are arranged so that their centroids lie on the transverse plane $x_2 = L_R$. The moment inferred from near surface stresses is

$$M_L^* = B \sum_{j=1}^{N_R} \left[\sigma_{22}^j l^j (x_1^j - h_R) + \sigma_{12}^j l^j L_R \right] \tag{4.12}$$

where B is the thickness of the specimen, N_R is the number of elements in the surface layer, x_1^j is the element centroid's x_1 coordinate and l^j is the length of the element in the x_1-direction. The normal and shear stresses σ_{22}^j and σ_{12}^j at the element's centroid are obtained by averaging the respective values at the eight Gauss points. The linearly interpolated normal stress changes its sign at $x_1 = h_R$. This defines the hinge axis for evaluating the M_R component (the first of two terms on the right side of (4.12)) of the inferred moment.

The rotation of the cracked section about the hinge axis, θ_L, is given by

$$\theta_L(t) = \delta(t) \Big/ (H - h_L(t)) \tag{4.13}$$

Here δ is the average of the opening displacements of the nodes at the crack mouth (along $x_1 = H$), and h_L is the hinge position (determined in connection with (4.11)) at time t. It may be noted that the opening displacement at the crack mouth vary negligibly with x_3. An inferred rotation, which is very useful from the point of view of dynamic fracture experiments, is θ_L^* given by

$$\theta_L^*(t) = \delta(t) \Big/ (H - h_L^*) \tag{4.14}$$

Here h_L^* is the hinge axis given by the slip-line field solution in [17]. In particular $h_L^*/b = 0.63$ which is very close to the hinge axis given by the finite element solution for the fully yielded state.

5. FINITE ELEMENT ANALYSIS

5.1 Computational model

The relative dimensions of the three-point-bend specimen are $L/H = 2.0$, $a/H = 0.5$, $B/H = 0.5$ and $L_T/H = 2.25$ where H is the width of the specimen, L is the length between the cracked section and the remote support, a is the crack length, B is the thickness and L_T is the half-length of the specimen (see Fig. 2a). These relative dimensions are in accord with ASTM specifications for the specimen for quasi-static fracture toughness evaluation. A typical dynamic fracture specimen has a width H equal to 2 inches and relative crack length a/H ranging from 0.4 to 0.7 [2].

Only a quarter of the three-point-bend specimen (region $x_2 \geq 0$, $x_3 \geq 0$) need be modeled since the problem possesses reflective symmetry with respect to the crack plane ($x_2 = 0$) and mid-plane ($x_3 = 0$). The finite element model of the quarter-specimen constructed with 8-node trilinear hexahedron (brick) elements is shown in Fig. 2b. Consider a layer of elements (one layer thick in the x_3 direction) which spans the x_1-x_2 plane. The element size in the x_1-x_2 plane is gradually increased with element distance from the crack plane. The identical planar mesh is repeated along the x_3-axis to form six layers of elements. To accomodate the anticipated strong variations of stresses and deformation (with respect to x_3) as the free surface is approached, the thickness of the elements is gradually reduced. The six layer of elements are bounded by the planes $x_3/B = 0.0,\ 0.17,\ 0.27,\ 0.35,\ 0.41,\ 0.46,\ 0.5$. The crack front is surrounded by six rings of specially arranged crack-tip elements. Each ring consists of four brick elements which are collapsed into wedges. The outermost ring at the free surface is shown in Fig. 2b. Displacement gradients within these elements contain terms of $O(1/r)$ in the x_1-x_2 plane [23] which nearly match the near-tip strain singularities associated with power-law hardening materials. The mesh has a total of 1692 elements (282 elements on each layer) and 2233 nodes.

On the plane of the uncracked ligament and mid-plane, normal displacements are prescribed to vanish. The model is roller-supported along the line $x_1 = H$, $x_2 = L$. A uniform pressure is applied over a quarter-region bounded by $0 \leq x_2 \leq H/8$ and $0 \leq x_3 \leq B/2$ on the plane $x_1 = 0$ so that the quarter-load is $P/4$. Twelve element surfaces constitute the plane of contact. At very early times, corresponding to the first few passes of the discrete waves across the length of the specimen, our calculations indicate that the specimen will lift off from its roller supports. However the imposed roller support conditions on the computational model did not allow for any motion in the x_1-direction. We did not refine our computational model to accomodate this phenomenon since the interval of interest to us falls far beyond the time where discrete wave effects are important.

The material behavior is taken to be governed by the J_2 flow (rate independent) theory of

plasticity. Under uniaxial stressing the material deforms according to

$$\begin{aligned} \epsilon/\epsilon_o &= \sigma/\sigma_o\,, \qquad \epsilon < \epsilon_o \\ \epsilon/\epsilon_o &= (\sigma/\sigma_o)^n\,, \quad \epsilon \geq \epsilon_o \end{aligned} \tag{5.1}$$

where σ_o and ϵ_o are the yield stress and strain related by $\sigma_o = E\epsilon_o$, E is Young's modulus and n is the strain hardening exponent. In our calculations, we have taken n to be 10 and Poisson's ratio ν to be 0.3, these values being representative of high-strength structural steels.

5.2 Dynamic Analysis

To obtain an estimate of the stable time step for the mesh depicted in Fig. 2b, we obtained the largest eigenvalue of the global elastic stiffness matrix. From this value, the dimensionless critical time step was determined to be $\Delta t\, c_1/H = 0.014$. Uniform time increments of $\Delta t\, c_1/H = 0.012$ was chosen for the entire simulation. The load applied at the mid-span increases linearly in the interval $0 < tc_1/H < 40$, and thereafter is kept constant at $PL/2M_0 = 1.2$ (see insert in Fig.6). This loading rate is representative of the nearly constant load application rate that has been achieved in three-point-bend bar fracture experiments through proper choice of impact absorber material [2]. Altogether 12000 uniform time increments were taken and the value of J and pertinent field quantities were evaluated at every 50 increments corresponding to a time interval of $tc_1/H = 0.6$. For this particular simulation, the CPU time expended on the Cray-XMP is about six hours.

We extracted J_{ave} and the value of J at each crack front node from finite element fields using the procedure discussed in Section 4.2. In the J calculations, values of q_2 and q_3 are prescribed to be zero everywhere in the domain since the normal to the (straight) crack front is in the x_1-direction. To calculate $\overline{J}_M$ using (4.2), q_1 is set equal to unity at the M^{th} node and zero at all other nodes on the crack front. Within a domain chosen for each calculation, the values of q_1 are in accord with the conditions given in Section 2.2 and further elaborated upon in Section 4.2. Four different domains were employed for the evaluation of $\overline{J}_M$. The smallest domain had twenty elements while the largest domain had more than four hundred elements. Typically the value of $\overline{J}_M$ associated with a domain is within two percent of its mean value. The near domain independence of $\overline{J}$ is an indication of the quality of the numerical solution. The mean value of $\overline{J}$ is used in (4.9) and (4.10) for the evaluation of J at the nodes and $J(s)$ at the point s on the crack front. We computed J_{ave} by integrating $J(s)$ along the crack front and then divide the result by the crack length. As a check, the average value is computed using (4.2) by taking q_1 to equal unity on all crack front nodes. The J_{ave} values determined by the two methods are exactly equal as they must be.

The increase of $J_{\text{ave}}/\sigma_o\epsilon_o a$ with time tc_1/H is plotted in Fig. 4. Also shown in the figure, is J at the symmetry plane ($x_3/B = 0$) and at the free surface ($x_3/B = 0.5$), denoted by J_{mid} and J_{edge} respectively. The local values at these two locations and all other crack front locations are determined using (4.10). Shown in Fig. 5 is the variation of J along the crack front at four different times. The local J values at each time have been normalized by the corresponding J_{ave}. The increasing through-thickness variation of J with the progress of time reveals the effect of plasticity which dominates the long time response of the specimen. Similar plasticity effects on three dimensional near tip fields have been observed in a quasi-statically loaded specimen [4].

The actual moment carried by the ligament M_L is calculated by (4.11). For subsequent discussion, we normalize M_L by the limit moment given by the plane strain rigid-perfectly plastic analysis [17]. The limit moment, M_o has the value $0.364\,\sigma_o b^2 B$ where σ_o is the yield stress, b is the ligament length and B is the thickness of specimen. The computed location of the effective hinge axis in the fully yielded state is very close to the location given in [17]. Plotted in Fig. 6 is the increase of the normalized moment M_L/M_o with dimensionless time tc_1/H. The effect of inertial screening is clearly evident at $tc_1/H < 20$. For times tc_1/H greater than about 20, the moment carried by the ligament rises rapidly. Beyond tc_1/H of about 40, M_L begins to level off and slowly approach the equilibrium moment. The rotation of the cracked section θ_L with time is nearly identical to that observed in the 2-D simulation of the same impact problem [1] and will not be discussed.

Through-thickness variation of the near tip stresses provide further insight into the 3-D nature of the fields. We examine the stresses on two lines parallel to the x_3-axis and located near to the crack front. Of particular interest in fracture initiation studies is the tensile stress σ_{22}. These stresses are evaluated at element centroids located at $r/H = 0.035, \theta = 27.3^o$ and $r/H = 0.099, \theta = 18.4^o$ where r and θ are the polar coordinates centered at the crack front and θ is measured from the crack plane. The through-thickness variation of σ_{22} (normalized by the yield stress σ_o) at four different times along the two line locations is shown in Fig. 7. At shorter times when the material responds elastically, the fields may be characterized as 2-dimensional. At longer times dominated by the plastic response of the material, the stresses develop strong through-thickness variation. This trend is similar to the variation of J along the crack front (see Fig. 5).

At the remote plane located approximately mid-way between the crack plane and roller supports ($x_2 = L/2$) there is hardly any variation of the axial stresses and the shear stresses through the thickness at all times, i.e., the fields may be characterized as plane stress. Furthermore the distribution of the normal strain and stress with x_1 is very nearly in agreement with the distribution according to elementary beam theory. It follows that the load carried by the ligament can be

inferred from surface measurements taken in the vicinity of the quarter-span. This is significant since this load is the input measurements for the application of the deep-crack formula for J. This will be taken up in the next section.

In the interval $0 < t < t_T$, the material response is elastic. At the transition time t_T elements immediately adjacent to the crack tip are partially yielded. As discussed in Section 3.2 it is doubtful that at this stage of the transient the near-tip fields are sufficiently established so that they can be characterized by J. At larger times the plastic zone emanating from the crack tip spreads across the ligament and joins up with the plastic zone emanating from the plane of impact. Effective stress contours at $tc_1/H = 144$ are shown in Fig. 8; the contour labeled by 1.0 is the boundary of the plastic zone. Plastic zone shape in the x_1-x_2 plane resembles the quasi-static plane strain plastic zone [16,23]. The extent of the plastic zone near the free surface ($x_3/B = \pm 0.5$) is larger than that at the mid-plane ($x_3/B = 0$) of the specimen.

To gain further insight into the behavior of the dynamically loaded specimen, results from the dynamic analysis are presented in a way that will allow a direct comparison with the quasi-static response of the specimen. First a quasi-static analysis based on the identical mesh is briefly discussed. A small load increment is applied so that the Gauss points nearest to the crack tip are on the verge of yielding. Thereafter the load increment is adjusted so that the plastic zone increases gradually. A total of 70 increments were taken to reach the final load of $M_L/M_o = 1.3$. On the average seven Newton-Raphson iterations were required to bring the imbalanced residual forces to a normalized error level of 10^{-5}.

Values of θ_L/ϵ_o and $J_{\text{ave}}/\sigma_o\epsilon_o a$ as functions of M_L/M_o as determined from the dynamic analysis are shown as solid line curves in Fig. 9a and 9b. The triangles are the results from a quasi-static analysis. The close agreement is indeed remarkable. Though not detectable in the plots, the quasi-static and dynamic values differ by about 20 percent at load level of $M_L/M_o = 0.1$; at even earlier times and lower loads the differences are larger. Plots of $J_{\text{ave}}/\sigma_o\epsilon_o a$ versus θ_L/ϵ_o for both dynamic and quasi-static cases are shown in Fig. 9c. We observe that with the appropriate normalizations, the relationship between normalized J_{ave} and normalized displacement (or rotation of the ligament), appear to be insenitive to loading rate in the regime dominated by structural inertial and deformation energy. A similar observation can be made on the relationship between J and the moment.

5.3 Comparison of (precise) J and J_{dc}

With the moment M_L (4.11) and the rotation θ_L (4.13) as the input measurements in (3.5), the value of J_{dc} as a function of time is obtained. For the purpose of appraising the accuracy of the

deep-crack J formula, the value of J_{dc} is divided by the average value, J_{ave}. The latter is the precise value determined from the computed field quantities using the domain integral expression (4.2). A ratio of unity represents perfect agreement between the deep-crack estimate and the precise value J_{ave}. The ratio J_{dc}/J_{ave} is plotted against tc_1/H in Fig. 10a. During the early transient, the ratio is substantially larger than unity, then falls below unity and starts to increase at about the transition time. It levels off at a value of 1.06 at about twice the transition time.

The ratio as a function of the actual moment carried by the ligament is shown by the solid line curve in Fig. 10b. We have noted that the actual moment carried by the ligament cannot be measured in an experiment, and a measurable moment was introduced Section 3.3. For this particular calculation, the measurable moment is determined by the fields at the free surface near to the quarter-span, $x_2 = 1.068H$. As discussed earlier the moment and shear force can be reliably determined from stresses near the surface at the chosen location since through-thickness variation of the fields near the quarter-span is negligible and the x_1-distribution of the numerically determined fields is nearly exactly given by elementary beam theory. Using the inferred moment M_L^* from (3.6) and θ_L^* from (4.14) in the deep-crack formula (3.5), a 'measurable' J_{dc} is obtained . This estimate of J normalized by the precise J_{ave} is shown by the dashed line curve in Fig. 10b. The agreement between the dashed line curve based on the 'measurable' moment and rotation, and the solid line curve based on the actual moment and rotation is quite good.

6. DISCUSSION

It has become fairly common practice to write the relationship between J and the work done on a specimen by the applied loads W as

$$J_{\text{ave}} = \eta\, W \,/\, (Bb) \tag{6.1}$$

where b is the length of uncracked ligament and Bb is the area of the uncracked ligament. In writing (6.1), we have followed the notation in this paper; in the published literature (particularly papers on fracture toughness measurements, e.g. [2]) the left hand side of (6.1) is usually written as J. Relationship (6.1) is a quasi-static loading deformation theory result and should provide an accurate estimate of J if proportional loading is nearly satisfied. For a deeply cracked bar, the values of 'eta factor' are available for remote loading ranging from pure stretch to pure bending [24]. The significance of the 'eta factor' is that it permits the the determination of J directly from the work done on the specimen by the applied load. Guided by (6.1), we introduce a similar 'eta factor' for transient loading defined by

$$\eta = J_{\text{ave}}\, B\, b \Big/ \int_0^{\theta_L(t)} M_L(t')\, d\theta_L(t') \tag{6.2}$$

where the integral in (6.2) is the work done *on the ligament* by the load M_L carried by the ligament (see Section 3.2). The variation of η with normalized moment is shown in Fig. 11 for times greater than the transition time. The solid line curve is determined from the results for present dynamic problem using (6.2). The triangles are values determined from finite element results for the quais-statically loaded specimen. While 'eta factor' varies negligibly with the applied moment in the quasi-static case (as it must), the value for the dynamic case starts at about 2.17 and decreases to about 1.95 for M_L/M_o equal to 1.2.

The transition time concept was introduced in [1] to provide an estimate of the range of time during which the crack tip field stabilizes and the deep-crack formula is applicable under transient loadings. In this paper, we have shown that the estimate of the transition time based on an elementary 2-D model analysis is in good agreement with the transition time obtained from the full-field 3-D transient solution (see Fig. 3). The usefulness of the concept for the particular class of dynamic fracture experiments being discussed is apparent from the plots in Figs. 10 and 11.

Full-field finite element simulation of a standard ASTM three-point-bend bar with relative crack depth 0.5 yields a transition time of about $24H/c_o$ (or $28H/c_1$). This time is roughly equal to the time required for the longitudinal wave to make six traverses of the span of the specimen,

or for the slower shear wave to make three passes. Indeed full-field calculations indicate that the fields have stabilized at times larger than twice the transition time. At such times the total kinetic energy is less than 20 percent of the total stress work on the body (see Fig. 3).

Similar observations concerning the transition from a response dominated by individual stress waves to a response dominated by the fundamental structural mode has also been discussed in a review paper by Ireland [25]. Ireland introduced an effective specimen inertial oscillation period, τ, and cited numerous experimental data which showed that inertial effects are dominant for times smaller than 2 τ. His proposed empirical relation for τ can be arranged in the form

$$\tau = 1.68 \times \sqrt{2}\ S\ \frac{H}{c_o} \tag{6.3}$$

where S is defined by (3.2). Based on the relative specimen dimensions employed in the present analysis, a value of τ equal to $23.8H/c_o$ is obtained from (6.3) which is remarkably close to the value we got from the finite element solution and the model analysis (3.1). Kalthoff [26] has also noted that elastic near-tip fields at short-times cannot be predicted by a static analysis. In the short-time transient regime ($t < 3\ \tau$), Kalthoff and coworkers (see publications referenced in [26]) advocate the use of impact response curves for estimating the dynamic stress intensity factor.

This study is directed at ductile materials where fracture initiation takes place after extensive yielding of the ligament has occured. Our analysis suggests that interpretable fracture toughness data can be obtained from dynamically loaded three-point-bend steel specimen if the time to fracture initiation is larger than about twice the transition time. In particular, the transition time for an ASTM three-point-bend steel specimen of width 5 cm (this dimension being typically denoted by W in the standards) and crack length to width ratio between 0.5 to 0.7 ranges from about 250 to 400 μs. Thus the time to fracture initiation should be greater than about 500 to 800 μs. Fracture initiation in ductile materials at much shorter times (less than 30 μs) can be achieved in the stress wave loaded cracked round bar experiment of Costin, Duffy and Freund [27]. A full-field transient finite element analysis of the fracture experiment has been carried out by Nakamura, Shih and Freund [28].

ACKNOWLEDGEMENTS

We are grateful for the research support of the Naval Sea Systems Command (SEA 05R15) through ONR grant N00014-85-K-0365, and the NSF Materials Research Laboratory at Brown University through Grant DMR83-16893.

The calculations reported on here were carried out in the VAX-11/780 Computational Facility at Brown University and on a Boeing Computer Services CRAY-XMP computer. The VAX facility was made possible by grants from the National Science Foundation (Solid Mechanics Program), the General Electric Foundation, and the Digital Equipment Corporation and access to the CRAY-XMP was made possible by the National Science Foundation.

REFERENCES

[1] T. Nakamura, C. F. Shih, and L. B. Freund, "Analysis of a dynamically loaded three-point-bend ductile fracture specimen," *Brown University Report* ONR0365/1 ,1985, in print *Engineering Fracture Mechanics,* 1986.

[2] J. A. Joyce and E. M. Hackett, "An advanced procedure for J-R curve testing using a drop tower," preliminary draft, November 1985.

[3] J. R. Rice, P. C. Paris and J. G. Merkle, "Some further results of J-integral analysis and estimates," in *Progress in flaw growth and fracture toughness testing,* ASTM STP 536, 1973, pp. 231-245.

[4] H. G. deLorenzi and C. F. Shih, "3-D elastic-plastic investigation of fracture parameters in side-grooved compact specmens," *International Journal of Fracture*, Vol. 21, 1983, pp. 195-220.

[5] M. Sakata, S. Aoki, K. Kishimoto and R. Takagi, "Distribution of crack extension force, the $\widehat{J}$-integral, along a through-crack-front of a plane," *International Journal of Fracture*, Vol. 23, 1983, pp. 187-200.

[6] C. F. Shih, B. Moran and T. Nakamura, "Energy release rate along a three-dimensional crack front in a thermally stressed body," *International Journal of Fracture*, Vol. 30, 1986, pp. 79-102.

[7] J. R. Rice, "A path independent integral and the approximate analysis of strain concentration by notches and cracks," *Journal of Applied Mechanics*, Vol. 35, 1968, pp. 379-386.

[8] D. M. Parks, "The virtual crack extension method for nonlinear material behavior," in *Computer Methods in Applied Mechanics and Engineering,* Vol. 12, 1977, pp. 353-364.

[9] T. K. Hellen, "On the Method of Virtual Crack Extension," *International Journal of Numerical Methods in Engineering* , Vol. 9, 1975, pp. 187-207.

[10] H. G. deLorenzi, "On the energy release rate and the J-integral for 3-D crack configurations," *International Journal of Fracture*, Vol. 19, 1982, pp. 183-193.

[11] F. Z. Li, C. F. Shih and A. Needleman, "A Comparison of methods for calculating energy release rate," *Engineering Fracture Mechanics*, Vol. 21, 1985, pp. 405-421.

[12] T. Nakamura, C. F. Shih and L. B. Freund, "Computational methods based on an energy integral in dynamic fracture," *International Journal of Fracture*, Vol. 27, 1985, pp. 229-243.

[13] J. K. Knowles and E. Sternberg, "On a Class of Conservation Laws in Linearized and Finite Elastostatics," *Archive for Rational Mechanics and Analysis*, Vol. 44, 1972, pp. 187-211.

[14] B. Budiansky and J. R. Rice, "Conservation laws and energy-release rates," *Journal of Applied Mechanics*, Vol. 40, 1973, pp. 201-203.

[15] B. Moran and C. F. Shih, "A general treatment of crack tip contour integrals," in preparation

[16] J. W. Hutchinson, "Fundamentals of the phenomenological theory of nonlinear fracture mechanics," *Journal of Applied Mechanics*, Vol. 50, 1983, pp. 1042-1051.

[17] A. P. Green and B. B. Hundy, "Initial plastic yielding in notch bend tests," *Journal of the Mechanics and Physics of Solids*, Vol. 4, 1956, pp. 128-144.

[18] G. L. Goudreau and J. O. Hallquist, "Recent developments in large-scale finite element lagrangian hydrocode technology," *Computer Methods in Applied Mechanics and Engineering*, Vol. 33, 1982, pp. 725-757.

[19] R. L. Taylor, "Computer procedures for finite element analysis," chapter in *The Finite Element Method*, authored by O. C. Zienkiewicz, McGraw-Hill(UK), London, England, 1977.

[20] J. C. Nagtegaal, D. M. Parks, and J. R. Rice, "On numerically accurate finite element solutions in the fully plastic range," *Computer Methods in Applied Mechanics and Engineering* , Vol. 4, 1974, pp. 153-178.

[21] T. J. R. Hughes, "Generalization of selective integration procedure to anisotropic and nonlinear media," *International Journal for Numerical Method in Engineering*, Vol. 16, 1980, pp. 1413-1418.

[22] O. C. Zienkiewicz, *The Finite Element Method*, McGraw-Hill(UK), London, England, 1977.

[23] N. Levy, P. V. Marcal, W. J. Ostergren and J. R. Rice, "Small scale yielding near a crack in plane strain : A finite element analysis," *International Journal of Fracture Mechanics*, Vol. 7, 1971, pp. 143-156.

[24] C. F. Shih and J. W. Hutchinson, "Combined loading of a fully plastic ligament ahead of an edge-crack," *Journal of Applied Mechanics*, Vol. 53, 1986, pp. 271-277.

[25] D. R. Ireland, "Critical review of instrumented impact testing," in *Proceedings of International Conference on Dynamic Fracture Toughness*, London, 1976, pp. 47-62.

[26] J. F. Kalthoff, "On the measurement of dynamic fracture toughness - a review of recent work" *International Journal of Fracture*, Vol. 27, 1985, pp. 227-298.

[27] L. S. Costin, J. Duffy and L. B. Freund, "Fracture initiation in metals under stress wave loading conditions," in *Fast Fracture and Crack Arrest,* ASTM STP 627, 1977, pp. 301-318.

[28] T. Nakamura, C. F. Shih and L. B. Freund, "Elastic-plastic analysis of dynamically loaded circumferentially notched round bar," *Engineering Fracture Mechanics*, Vol. 22, 1985, pp. 437-452.

FIGURE CAPTIONS

Fig. 1 (a) Crack tip contour Γ inscribed on the plane locally perpendicular to the crack front where s is the arclength, (b) virtual crack advance within s_a and s_b represented by $l_k(s)$, (c) unit normal m_i pointing 'away' from volume enclosed by $\mathcal{S}_t$, $\mathcal{S}_+$, $\mathcal{S}_-$ and $\mathcal{S}_o$.

Fig. 2 (a) Schematic of three-point-bend specimen. The global coordinates x_1, x_2 and x_3 are indicated. (b) Finite element model of quarter-specimen.

Fig. 3 Ratio of total kinetic to deformation energies as determined from an elementary elastic model analysis. For comparison the finite element results are included. The transition time t_T is indicated.

Fig. 4 Behavior of J_{ave}, and local $J's$ at the mid-point and the edge of the crack front.

Fig. 5 Variation of J along crack front at four different times. The pointwise J values are normalized by the corresponding J_{ave}.

Fig. 6 Moment carried by ligament plane as a function of elapsed time. The applied load is shown in insert.

Fig. 7 Through-thickness variations of normal tensile stress σ_{22}. The locations of the two lines (parallel to the x_3-axis are (a) $x_1/H = 0.469$, $x_2/H = 0.016$ ($r/H = 0.035$, $\theta = 27.3^o$), (b) $x_1/H = 0.406$, $x_2/H = 0.031$ ($r/H = 0.099$, $\theta = 18.4^o$).

Fig. 8 Effective stress contours for $\sigma_e/\sigma_o = 0.8, 1.0, 1.2, 1.3$, at $tc_1/H = 144$.

Fig. 9 Relationships between moment carried by ligament, rotation of cracked section and J_{ave}. Static results shown by the triangles are included for comparison.

Fig. 10 Comparison of J_{dc} with J_{ave} (a) as a function of time, (b) as a function of moment carried by ligament. The dashed line is based on measurable moment and rotation.

Fig. 11 Dependence of 'eta factor' on moment carried by ligament for times greater than the transition time. Values for the quasi-statically loaded specimen are shown by the triangles.

Fig. 1

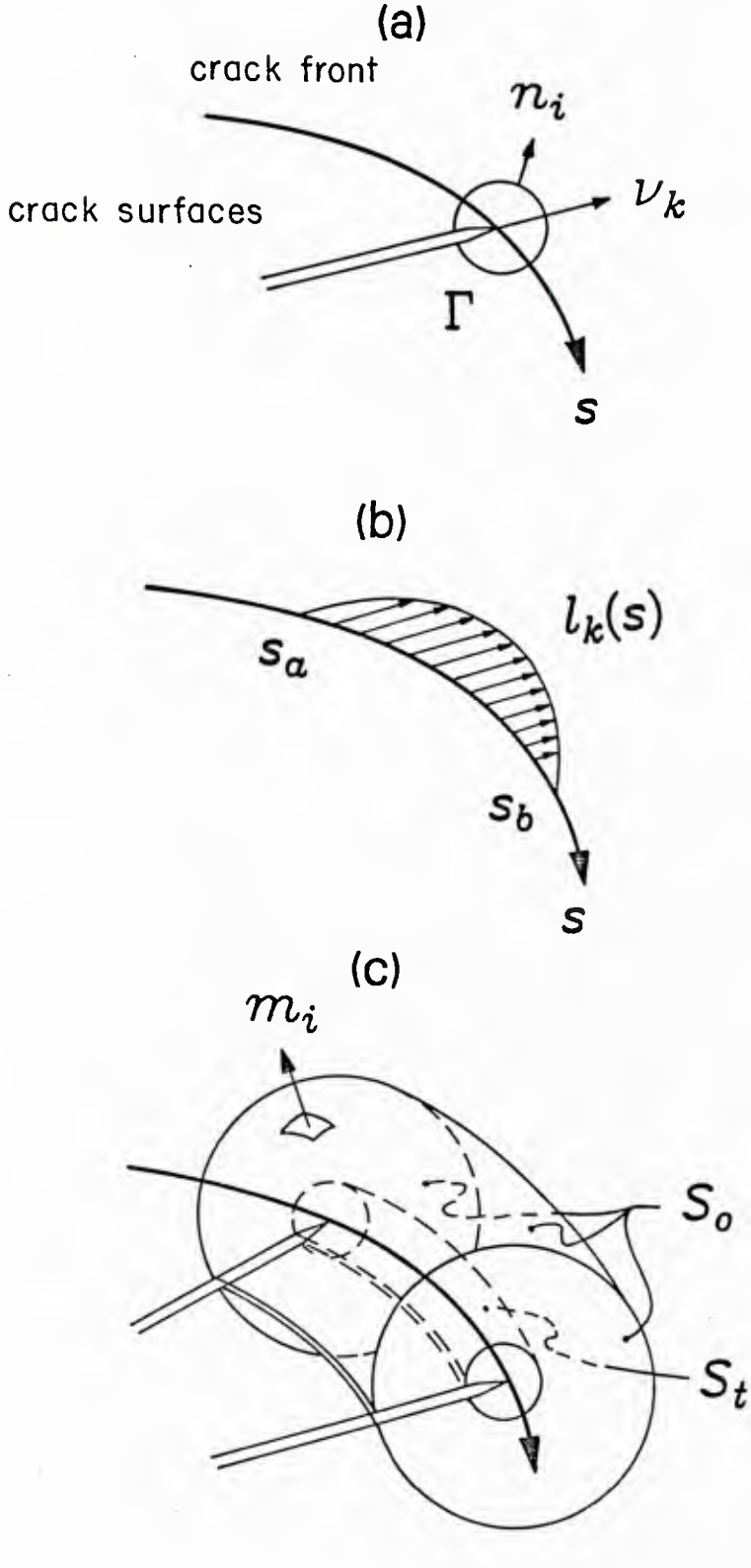
(a)
crack front
n_i
crack surfaces
ν_k
Γ
s
(b)
$l_k(s)$
s_a
s_b
s
(c)
m_i
S_o
S_t

Fig. 2

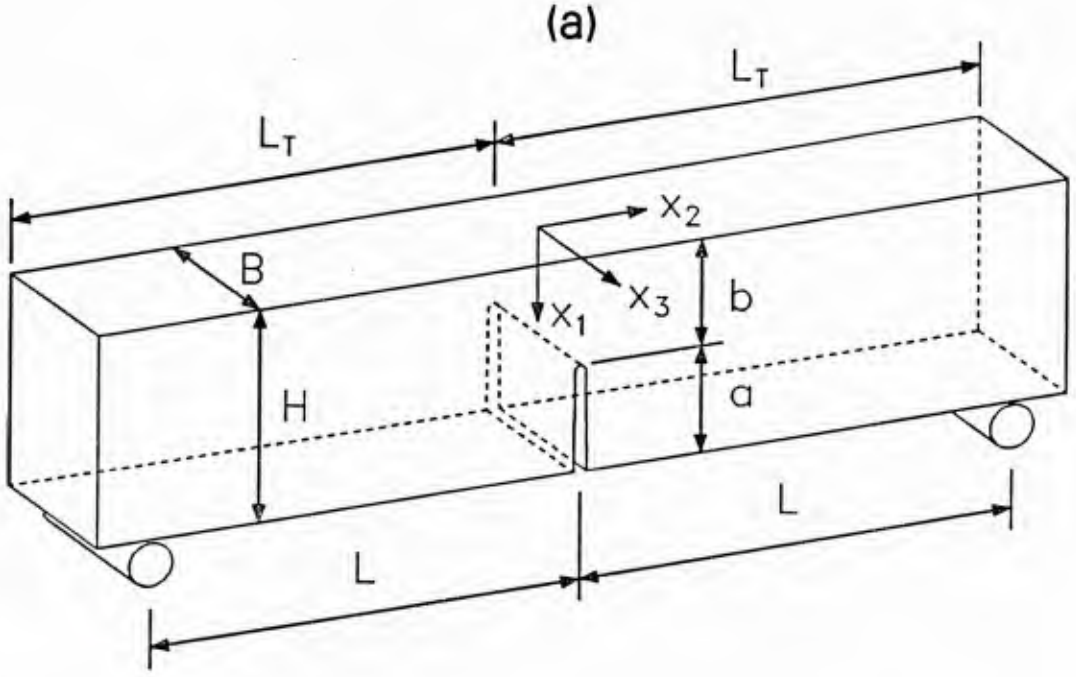

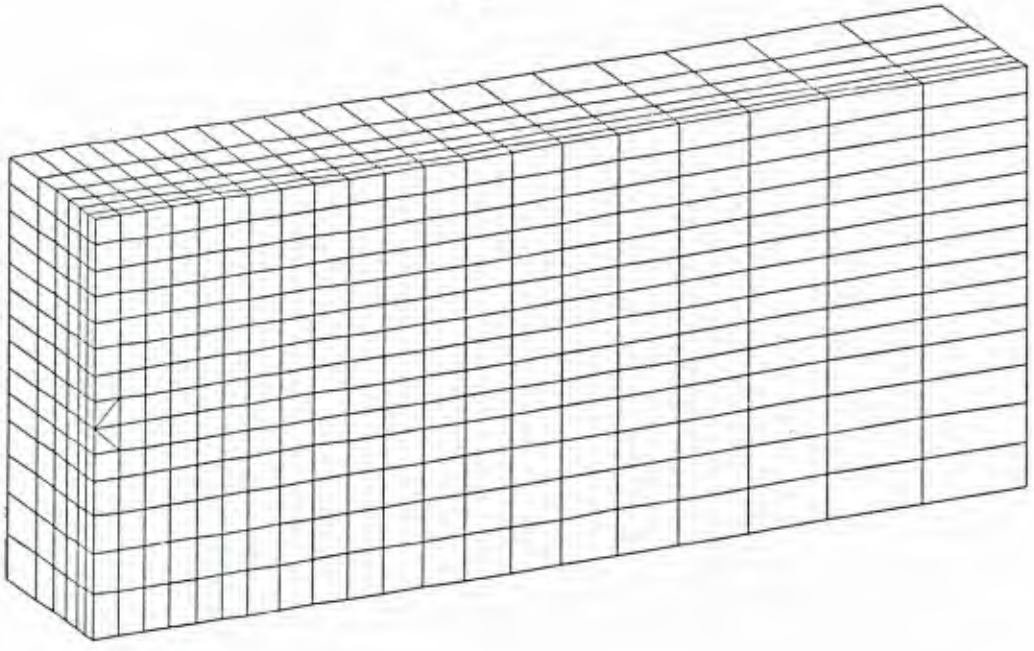

Fig. 3

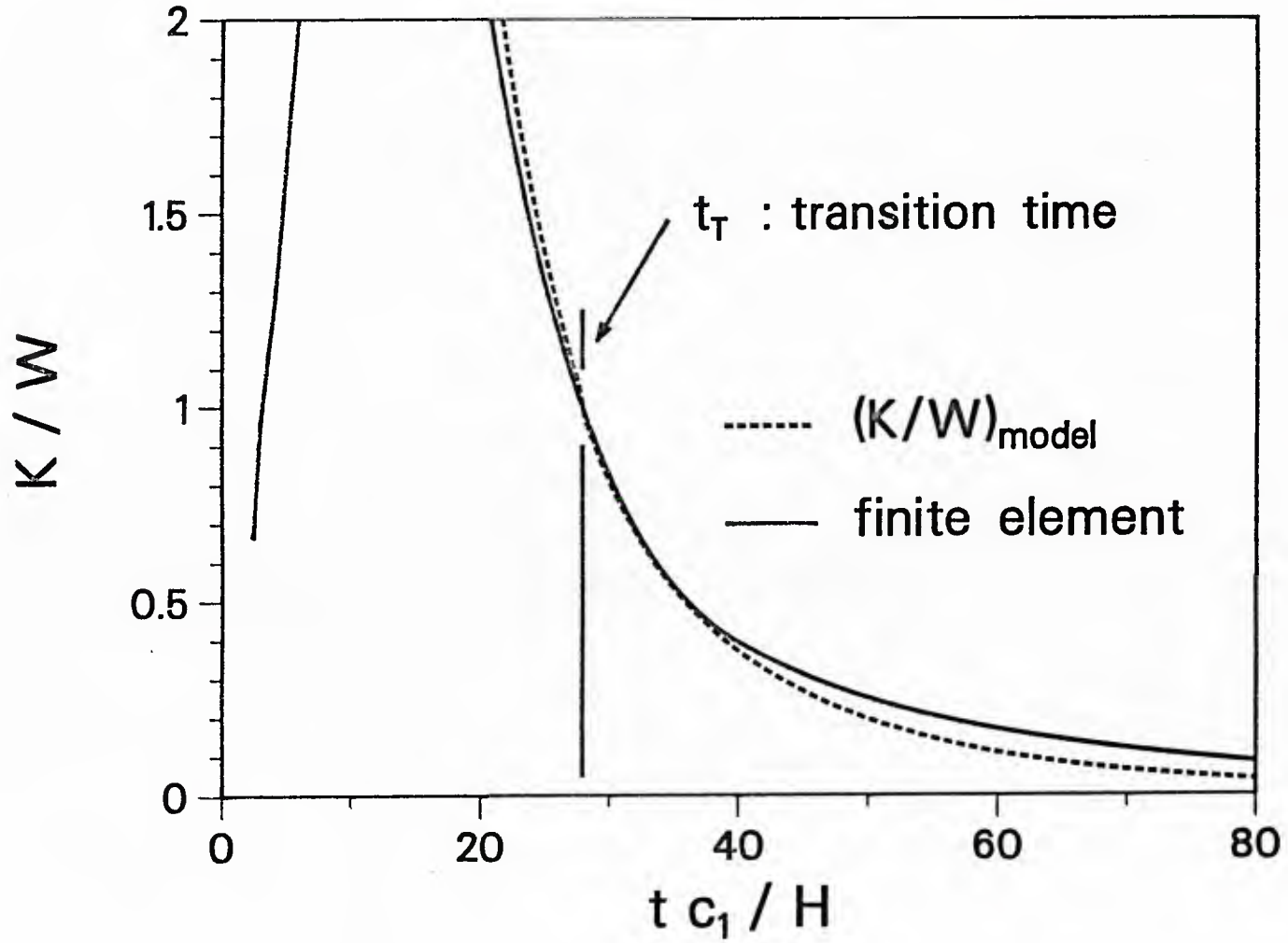
2
1.5
1
0.5
0
K / W
0
20
40
60
80
t c1 / H
tT : transition time
(K/W)model
finite element

Fig. 4

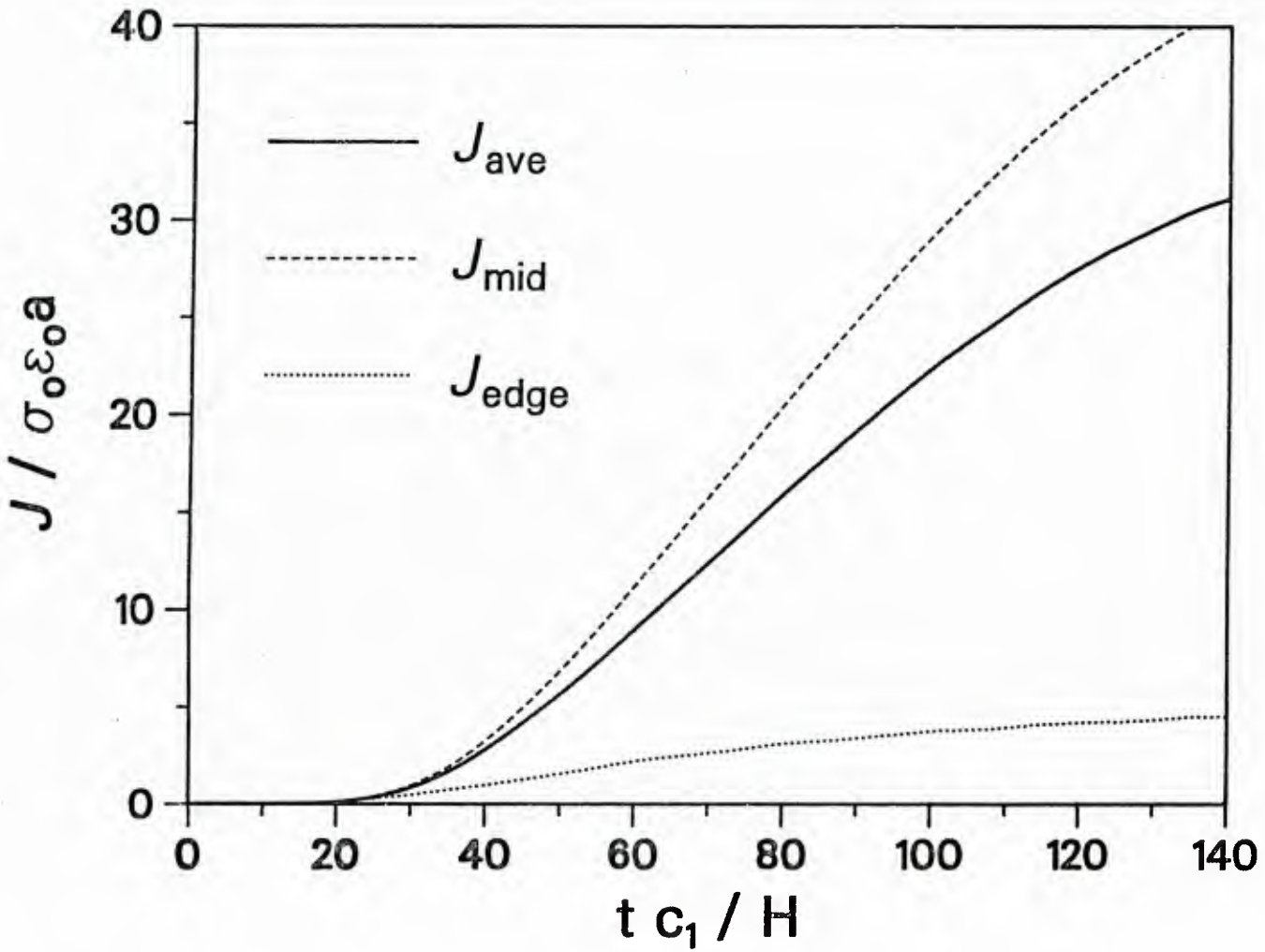
40
30
20
10
0
0
20
40
60
80
100
120
140
J_{ave}
J_{mid}
J_{edge}
$J / \sigma_o \varepsilon_o a$
$t\ c_1 / H$

Fig. 5

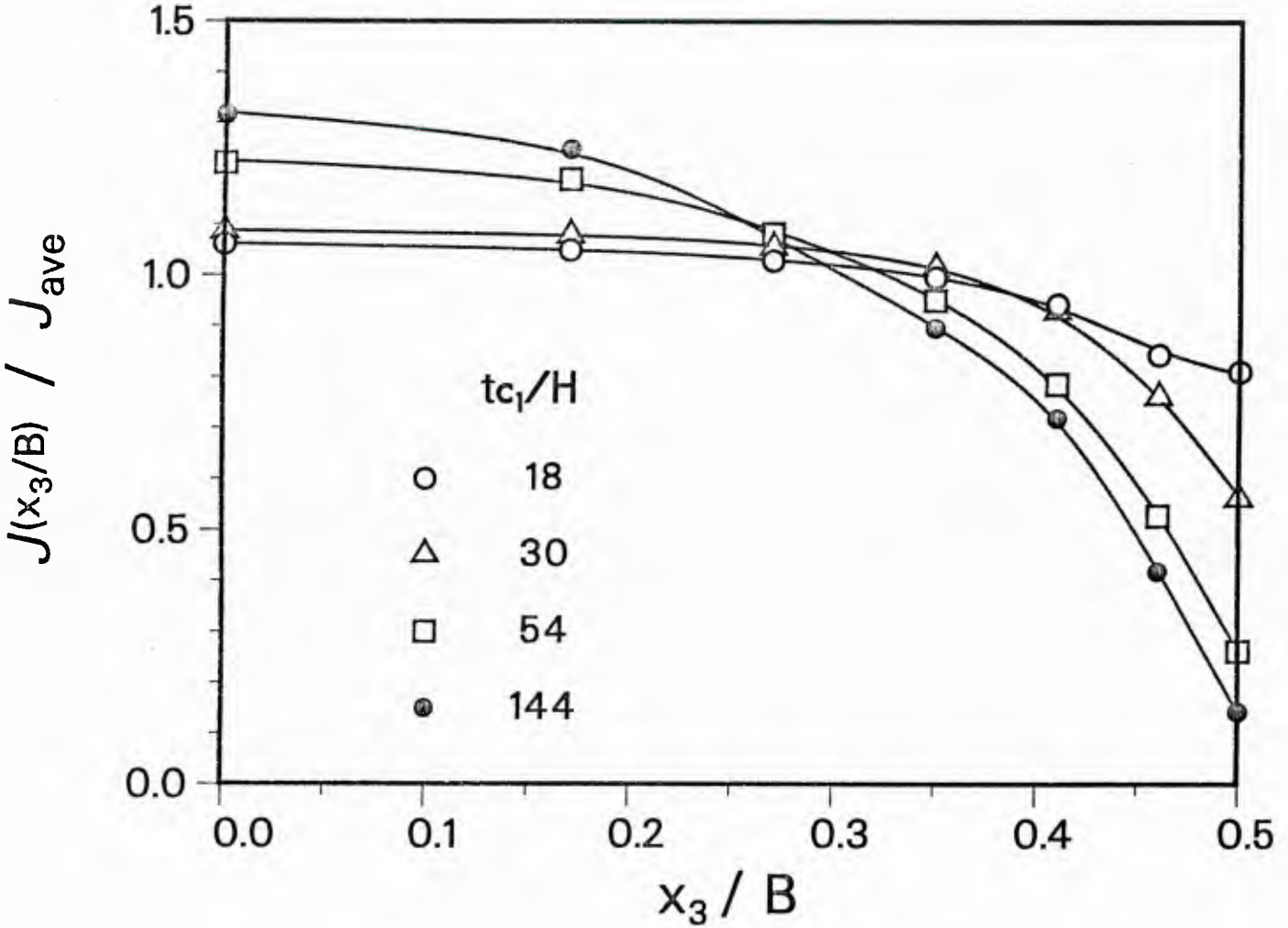

Fig. 6

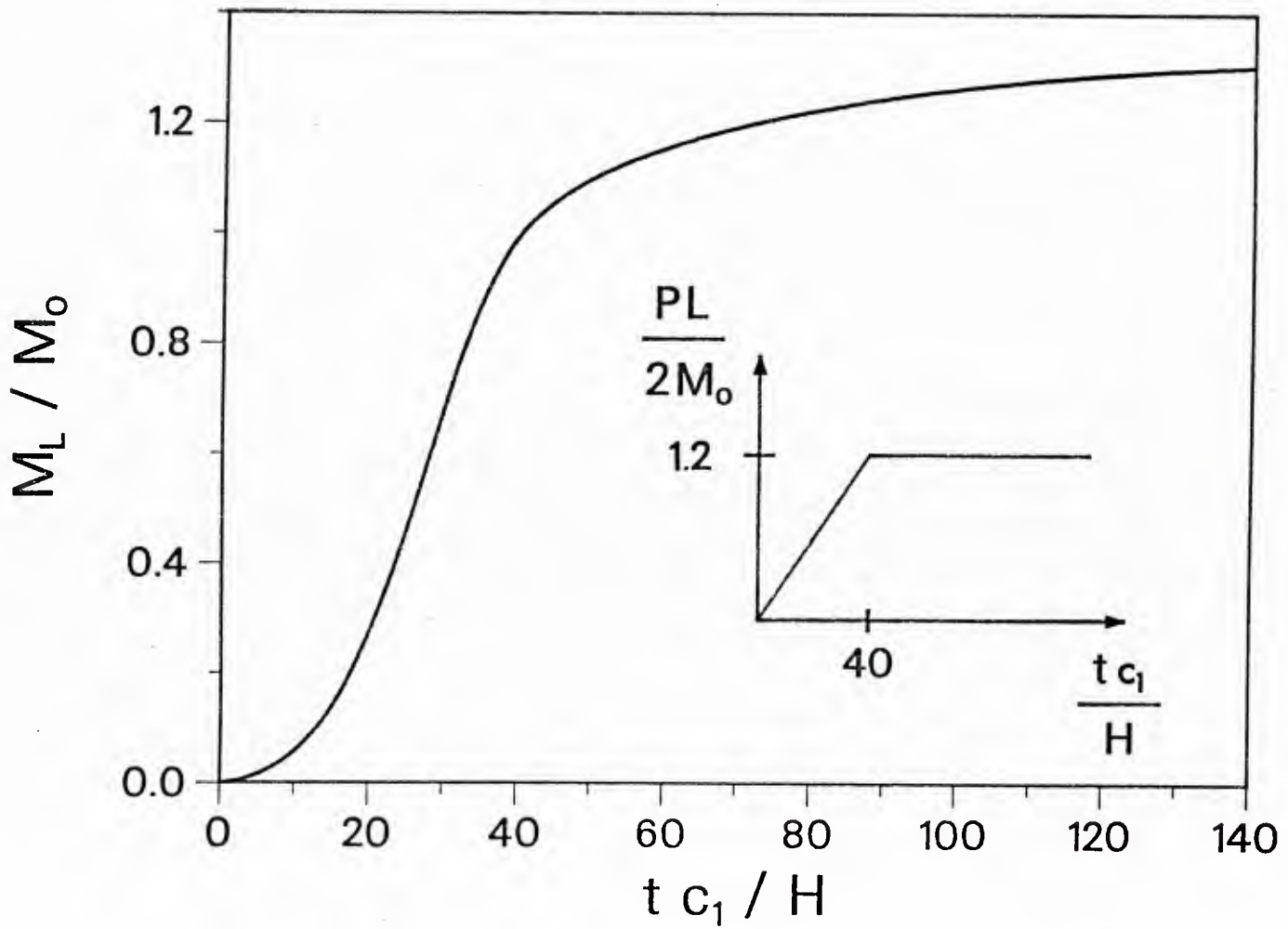
1.2
0.8
0.4
0.0
M_L / M_o
0
20
40
60
80
100
120
140
$t\,c_1 / H$
$\frac{PL}{2M_o}$
1.2
40
$\frac{t\,c_1}{H}$

Fig. 7

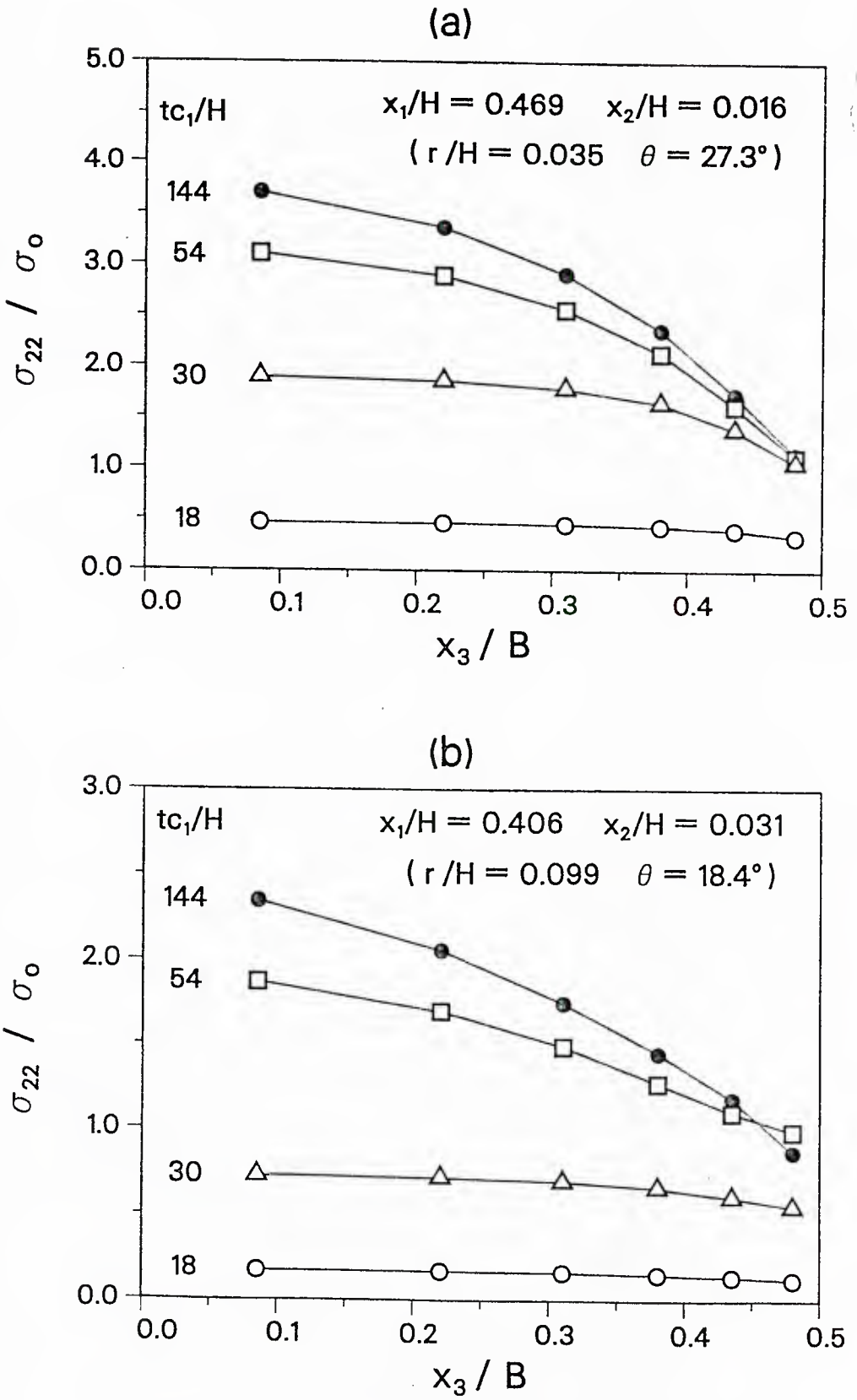
(a)
5.0
4.0
3.0
2.0
1.0
0.0
σ_{22} / σ_o
tc_1/H
$x_1/H = 0.469$ $x_2/H = 0.016$
(r /H = 0.035 $\theta = 27.3°$)
144
54
30
18
0.0
0.1
0.2
0.3
0.4
0.5
x_3 / B
(b)
3.0
2.0
1.0
0.0
σ_{22} / σ_o
tc_1/H
$x_1/H = 0.406$ $x_2/H = 0.031$
(r /H = 0.099 $\theta = 18.4°$)
144
54
30
18
0.0
0.1
0.2
0.3
0.4
0.5
x_3 / B

Fig. 8

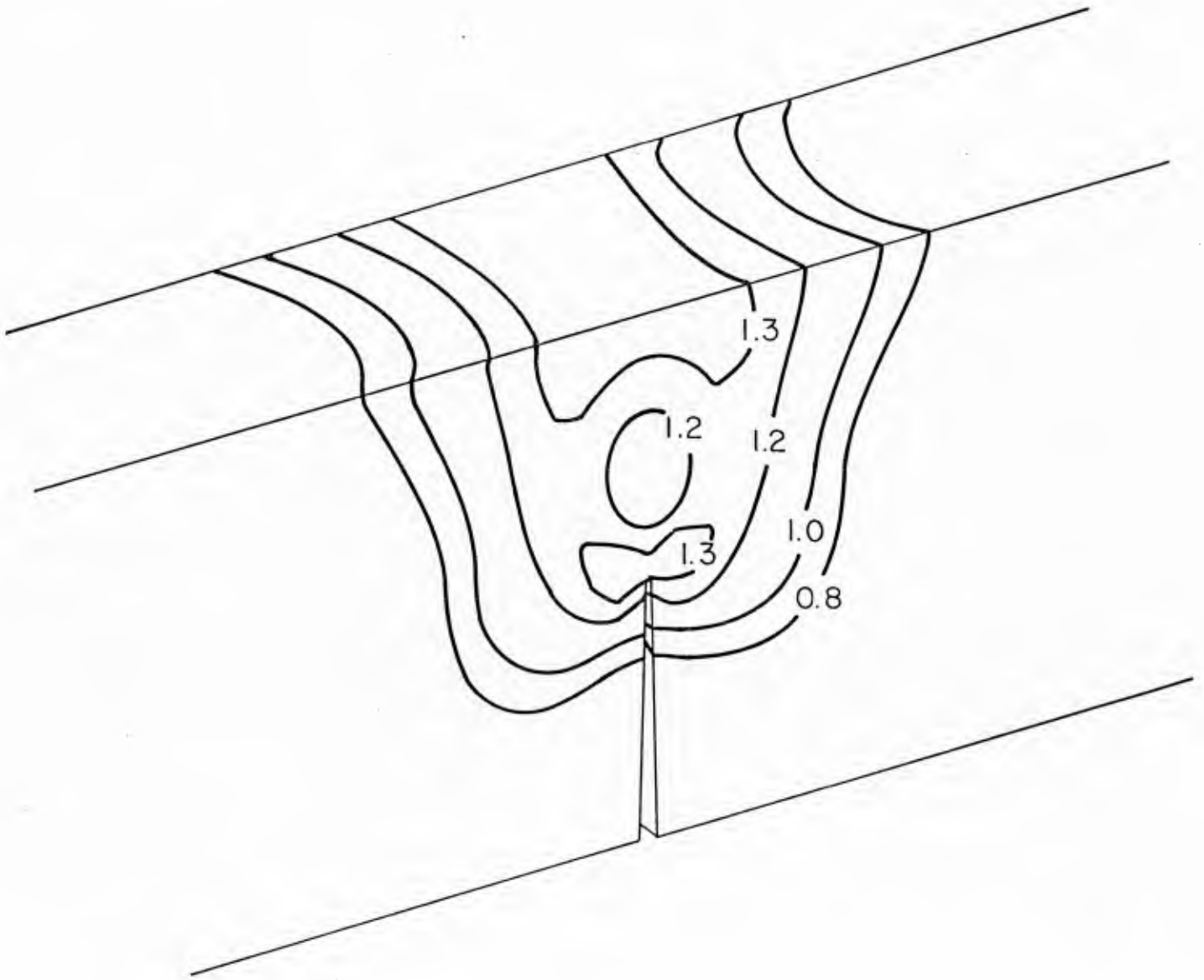

Fig. 9

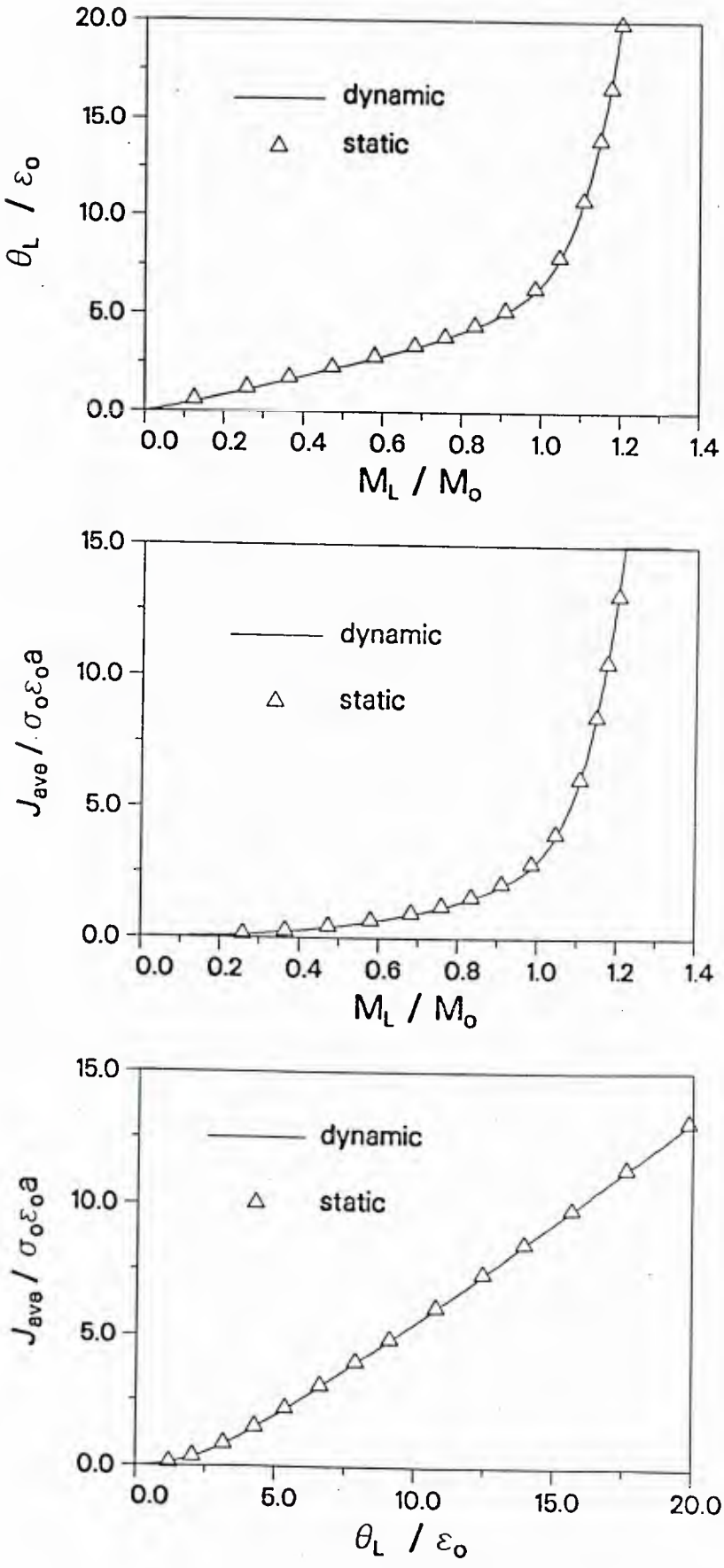
20.0
15.0
10.0
5.0
0.0
dynamic
static
θ_L / ε_o
0.0 0.2 0.4 0.6 0.8 1.0 1.2 1.4
M_L / M_o
15.0
10.0
5.0
0.0
dynamic
static
$J_{ave} / \sigma_o \varepsilon_o a$
0.0 0.2 0.4 0.6 0.8 1.0 1.2 1.4
M_L / M_o
15.0
10.0
5.0
0.0
dynamic
static
$J_{ave} / \sigma_o \varepsilon_o a$
0.0 5.0 10.0 15.0 20.0
θ_L / ε_o

Fig. 10

(a)

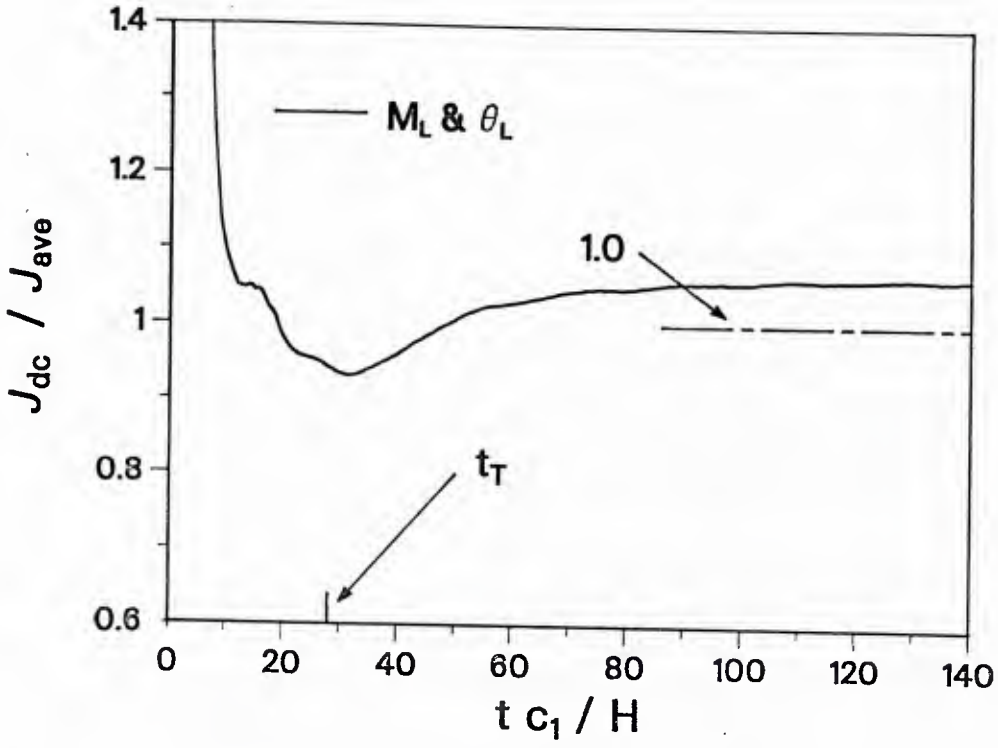
1.4
1.2
1
0.8
0.6
J_{dc} / J_{ave}
M_L & θ_L
1.0
t_T
0
20
40
60
80
100
120
140
t c_1 / H

(b)

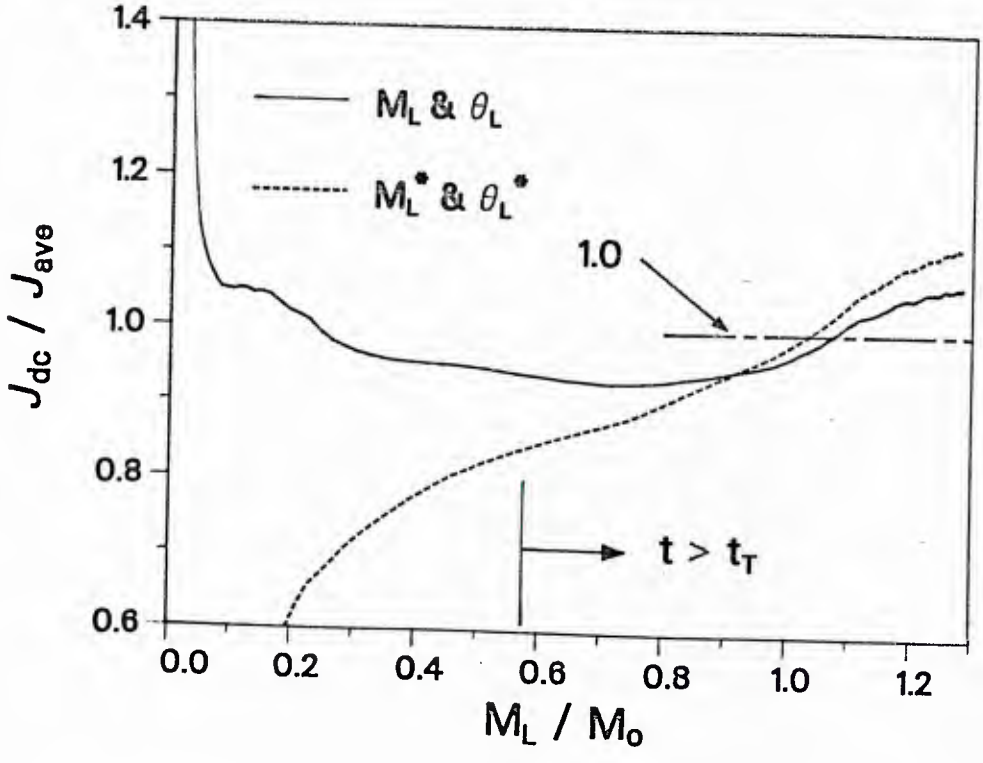
1.4
1.2
1.0
0.8
0.6
J_{dc} / J_{ave}
M_L & θ_L
M_L^* & θ_L^*
1.0
t > t_T
0.0
0.2
0.4
0.6
0.8
1.0
1.2
M_L / M_o

Fig. 11